Fe(II) and tannic acid-cloake MOF as carrier of artemisinin for supply of ferrous ions to enhance treatment of triple-negative breast cancer

Zihaoran Li
Weifang Medical University
Xinghan Wu
Weifang Medical University
Wenyu Wang
Weifang Medical University
Chengcheng Gai
Weifang Medical University
Wei-Fen Zhang
Weifang Medical University
Wentong Li
Weifang Medical University
Dejun Ding (dejunding@wfmc.edu.cn)
Weifang Medical University https://orcid.org/0000-0001-7809-7963

Nano Express

Keywords: Artemisinin, Ferroptosis, Triple-negative breast cancer, Metal organic frameworks, Reactive oxygen species,

Posted Date: September 25th, 2020

DOI: https://doi.org/10.21203/rs.3.rs-77012/v1

Version of Record: A version of this preprint was published on February 23rd, 2021. See the published version at https://doi.org/10.1186/s11671-021-03497-z.

Abstract

Suppression of tumor development by inducing ferroptosis may provide a potential remedy for triple-negative breast cancer (TNBC), which is sensitive to intracellular oxidative imbalance. Recently, artemisinin (ART) and its derivatives have been investigated as potential anticancer agents for the treatment of highly aggressive cancers via the induction of ferroptosis by iron-mediated cleavage of the endoperoxide bridge. Poor water solubility and insufficient availability of intracellular ferrous ions, limit the further application of ART in antitumor therapy. In this study, ferrous-supply nanocarrier was constructed based on tannic acid (TA) and ferrous ion (Fe^{2+})-coated on the zeolitic imidazolate framework-8(ZIF) with ART encapsulated (TA-Fe/ART@ZIF). via supramolecular coordination. Following the internalization of the as-prepared nano-system in cells, acidic degradation of the vehicles would facilitate the release of ART and accumulation of Fe^{2+}. The results revealed that the newly developed nano-drug system displayed a high level of intracellular ROS generation, and markedly enhanced ferroptosis. This work provides a novel approach to enhance the potency of ferroptotic nanomedicine and new directions for TBNC therapy.

Introduction

Ferroptosis, a newly discovered subtype of cell death, can result in accumulation of iron-dependent lipid hydroperoxides (LPO), leading to damage of the cell structure and integrity.[1-3] Emerging evidence implied that activation of ferroptosis by several small molecules is an effective approach for tumor suppression in various experimental cancer models, and created high expectations for the potential of ferroptosis as a novel anti-cancer therapy.[4-6] Triple-negative breast cancer (TNBC) is the most aggressive subtype of breast cancer lacking targeted therapies, and often associated with tumor recurrence, distant metastasis, and resistance to therapy.[7] Previous studies have pointed out that xCT cystine/glutamate antiporter is highly expressed in numerous TNBC cells, playing an important role in maintaining the glutathione (GSH) levels and redox balance. [8] Reduction of the intracellular GSH content can render TNBC cells sensitive to ferroptosis, thereby killing tumor cells.[8] Notably, ferroptosis can also bypass the resistance of TNBC to routine programmed apoptosis.[9] Therefore, strategies or drugs based on inducing ferroptosis may have therapeutic potential for the clinical treatment of refractory TNBC.

Artemisinin (ART), a sesquiterpene lactone that contains a peroxide group, was isolated from the traditional Chinese plant *Artemisia annua* and has demonstrated desirable antitumor activity in multiple cancer cell lines.[10,11] Increasing evidence displayed that cancer cells contain significantly more intracellular iron pool than normal cells, while iron-mediated cleavage of the endoperoxide bridge allows ART to selectively cause cell death in multiple cancer cell lines.[12,13] The iron ion-depended antitumor activity has attracted increasing attention on ART-regulated ferroptosis, an iron-dependent cell death.[13] Mechanistically, ART can induce lysosomal degradation of ferritin in an autophagy-independent manner, increasing the cellular levels of ferrous ion and sensitizing cells to ferroptosis.[11]

However, whether ART induces ferroptosis in TNBC remains unclear. In addition, a series of factors, such as poor water solubility and insufficient availability of intracellular ferrous ions, limit the further application of ART in antitumor therapy.[13] ART prodrug nanocomplexes are expected to be successfully used as a prospective nano-drug delivery system for ART-based anti-tumor drugs.[14-16] In recent years, metal organic frameworks (MOFs) have been prominently used in the field of biomaterials. As a representative of MOF-type materials, the zeolitic imidazolate framework (ZIF-8) is widely used in the development of nanomedicines with characteristics of pH-responsiveness, high drug loading, and good biocompatibility.[17-19] Furthermore, the ability to incorporate an adjustable surface on MOF permits the control of surface properties and its endowment with multifunctionalities.[20,21] The supramolecular assembly of a metal-phenolic coordination coat on the MOF surface has recently attracted interest owing to the desirable properties, such as stimuli-responsive disassembly, colloidal stability, and biocompatibility.[22,23] The metal-phenolic coordination materials on the MOF could be an ideal vehicle for delivering the hydrophobic ART.

Inspired by this, we developed ferrous ion -tannic acid coordination cloaked ZIF-8 nano-system encapsulating ART (TA-Fe/ART@ZIF) for regulating ferroptosis in TNBC cells, which is demonstrated in Fig. 1. ZIF-8 was selected as a nanocarrier to encapsulate ART owing to its high drug loading, good biocompatibility and pH- responsive release. The ferrous ion -TA coordination coat was immobilized onto the surface of ART@ZIF for the purpose of dispersion stability and supply of ferrous ions (Fe^{2+}). Following the internalization of the as-prepared nanosystem in cells, acidic degradation of the vehicles would facilitate the release of ART and accumulation of Fe^{2+}. The upregulation of Fe^{2+} levels in cells would decompose ART into radicals through cleavage of the iron-mediated endoperoxide bridge, markedly enhancing the effects of ferroptosis. Conclusively, the discovery of TA-Fe/ART@ZIF-mediated ferroptosis may offer new perspectives for the development of novel treatments against TNBC.

Materials And Methods

Reagents

Artemisinin (99%), 2-methylimidazole (98%), zinc nitrate ($ZnNO_3$; 98%), Ta (98%), ferrous sulfate ($FeSO_4$; 98%), and anhydrous methanol were provided by Aladdin-Reagent Co. Ltd. (Shanghai, China).

Fabrication of TA-Fe/ART@ZIF nanoparticles

For the preparation of Art nanoparticles, 200 mg of Art was dissolved in 1 mL of anhydrous methanol, and 2 g of 2-methylimidazole (the solvent was 8 mL of absolute methanol) was slowly added to the obtained Art solution. Under magnetic stirring, 0.2 g of zinc nitrate (the solvent was 1 mL of absolute methanol) was slowly added. Finally, the volume of the solution was adjusted to 15 mL and stirred for 10 min to obtain a light white solution. After centrifugation at 10,000 rpm, the sample was washed thrice with methanol. The supernatant from the first centrifugation was maintained to measure the content of Art, while the precipitant was freeze dried to obtain solid state for further use.

For the preparation of TA-Fe/ART@ZIF nanoparticles, 40 mg of solid Art nanoparticles was dissolved in water (1 mL). Ta (80 mg) (Ta solvent was 2 mL of deionized water) was slowly added to the nanoparticle solution and the volume of the solution was adjusted to 76 mL. After stirring for 20 min, 20 mg of $FeSO_4$ (the solvent was 4 mL of deionized water) was slowly added to the solution. After repeated stirring for 30 min, a dark purple solution was obtained. The solution was centrifuged at 10,000 rpm, washed thrice with water, and the precipitant was freeze dried to obtain solid statefor further use TA-Fe/ART@ZIF.

Transmission electron microscopy (TEM) and dynamic light scattering analysis of TA-Fe/ART@ZIF nanoparticles

TEM (JEM-1230; JEOL,Tokyo, Japan) was used to determine the morphological and elemental composition of each part of the nanoparticle. Dynamic light scattering and zeta potential (DLS; Zetasizer Nano system Malvern Instruments, Malvern, United Kingdom) were used to evaluate the particle size and electrical stability of the nanoparticles.

Fourier transform infrared spectroscopy (FTIR) and thermogravimetric analysis of TA-Fe/ART@ZIF nanoparticles

Fourier transform infrared spectroscopy (VERTEX 70; Bruker, Bremen, Germany) and thermogravimetric analysis were used to analyze the composition of the constituents of the nanoparticles.

Measurement of encapsulation efficiency and loading capacity

High-performance liquid chromatography (HPLC) (Agilent 1200; *Agilent* Technologies, Santa Clara, CA.) was used to measure the amount of Art in the supernatant. The drug loading and encapsulation rates of ART can be calculated as follows:

$$\text{Drug loading}\ (\%)=\frac{\text{Actual amount of drug encapsulated in NPs}}{\text{Amount of NPs}}\times 100\%$$

$$\text{Entrapment efficiency}\ (\%)=\frac{\text{Actual amount of drug encapsulated in NPs}}{\text{Initial of amount of drug used}}\times 100\%$$

In vitro release and pH-response of TA-Fe/ART@ZIF nanoparticles

The treated dialysis membrane wrapped with 2 mg of nanoparticles was placed in 50 mL of phosphate-buffered saline (PBS) with pH of 7.4 and 5.0, respectively, and shaken continuously at 37°C. The solution outside the dialysis membrane was sampled at 15 min, 30 min, 45 min, 1 h, 2 h, 4 h, 6 h, 8 h, and 10 h after the initiation of the experiment. The contents of Art in the buffer solution were measured using HPLC.

Cell culture

MDA-MB-231 and L929 cell lines were acquired from the American Type Culture Collection (American TypeCulture Collection, Manassas, VA, USA). Cells were cultured at 37°C and 5% CO_2 humidity in RPMI-1640 medium (Solarbio, Beijing, China), which was supplemented with 10% fetal bovine serum (Cyclone,Utah, USA), 100 μg/mL of sodium pyruvate, penicillin, and streptomycin (Solarbio Beijing, China).

Cellular toxicity test in vitro

Cell viability was determined using 3-(4, 5-Dimethylthiazol-2-yl)- 2,5-diphenyltetrazolium bromide (MTT) assay (Beyotime Biotechnology, Nanjing, China). MDA-MB-231 cells and L929 cells were cultured in standard cell media in 96-well plates (5,000 cells per well) and incubated in 5% CO_2 at 37°C for 24 h. The fluid in the well was discarded, and 100 μL per well of the serum-free medium with PBS and different concentrations of ART, TA-Fe/ZIF, TA-Fe/ART@ZIF, deferoxamine (MedChemExpress, Shanghai, China), N-benzyloxycarbonyl-Val-Ala-Asp(O-Me) fluoromethyl ketone (Z-VAD-FMK; MedChemExpress), and ferrostatin-1 (MedChemExpress) were added to the 96-well plates. After 48 h, 10 μL of MTT (5 mg/mL) was added and incubated for 4 h. Finally, an automatic enzyme marker (BioTek Instruments Inc., USA) was used to measure the absorbance in each well. Results were expressed as the percentage of cell viability.

Calcein-acetoxymethyl (Calcein-AM) staining assay

MDA-MB-231 cells were cultured in 24-well plates (2×10^4 cells per well) and incubated for 24 h. Subsequently, the cells were treated with different concentrations of TA-Fe/ART@ZIF nanoparticles for 24 h. After discarding the medium, the cells were stained with Calcein-AM (Beyotime Biotechnology, Shanghai, China) in the dark at 4°C for 20 min and observed under a fluorescence inverted microscope (Olympus, Tokyo, Japan).

Flow cytometry for apoptosis

MDA-MB-231 cells were placed in a six-well plate at a density of 2.5×10^5 cells per well under the same conditions. After treatment with PBS, ART, TA-Fe/ZIF, and TA-Fe/ART@ZIF were applied for 24 h. Subsequently, the cells were centrifuged and collected from the six-well plate. After propidium iodide and Annexin-V double staining (Annexin V-FITC Kit; Beckman Coulter, Marseille, France), flow cytometry was used to detect.

In vitro reactive oxygen species (ROS) determination assay

The determination of ROS content in cells was performed using a ROS fluorescence probe (dichloro-dihydro-fluorescein diacetate [DCFH-DA]; Beyotime Biotechnology, Shanghai, China). MDA-MB-231cells were cultured into six-well plates (2.5×10^5 cells per well) and incubated in 5% CO_2 at 37°C for 24 h. The fluid from the wells was discarded, and cells were treated as follows: blank control group (serum-free medium), positive control group and experimental group (different concentrations of nanoparticles).

Following incubation for 8 h at 37°C, 0.1% DCFH-DA was added to each well and the cells were incubated for 30 min. Cells unresponsive to DCFH-DA were removed with PBS and observed under a fluorescence inverted microscope (Olympus, Tokyo, Japan).

Malondialdehyde (MDA) and GSH content determination

The MDA assay kit (TBA method; Jiancheng Bioengineering, Nanjing, China) and GSH assay kit (Beyotime Biotechnology, Shanghai, China) were used to measure the intracellular levels of MDA and GSH. After treatment with PBS, ART, TA-Fe/ZIF and TA-Fe/ART@ZIF, MDA-MB-231 cells were collected and counted. The intracellular content of MDA and GSH was determined according to the instructions provided in the kits.

Western blot analysis

The MDA-MB-231 cells which treated with different nanoparticles were lysed with RIPA lysis buffer. After the protein concentration was determined, the proteins of different samples were separated using 10% SDS-PAGE gel and transferred to nitrocellulose membrane. The nitrocellulose membrane which loaded with sample proteins was blocked by 0.5% BSA protein solution for 1 h, and the nitrocellulose membrane and the primary antibodies were incubated for 24 h at 4°C. We rinsed the primary antibodies from the nitrocellulose membrane with TBST and continued to place it with the corresponding secondary antibodies at ordinary temperature for 2 hours. After washing off the secondary antibodies on the in cellulose membrane, the nitrocellulose membrane was used a chemiluminescent solution and observed under the gel imaging system.

Statistical analysis

All experiments were repeated at least thrice. All data were statistically analyzed using the SPSS version 22.0 software (IBM Corp., Armonk, USA). The results were expressed as the mean ± standard deviation. P-values <0.05 denoted statistical significance.

Results And Discussion

Characterizations of Art@TaFe-Zif nanoparticles

First of all, the ART@ZIF nanoparticles were synthesized at room temperature from methanol, zinc acetate, ART, and 2-methylimidazole according to literature procedures.[24] Stable metal-polyphenol supramolecular films were then rapidly formed around the ART@ZIF templates by vortexing TA and ferrous ions. The encapsulation efficiency, which was measured by HPLC using the supernatant from the first centrifugation was 66.7%. The supernatant was obtained the TA-Fe/ART@ZIF nanoparticles and the calculated drug load of Art was 11.4%. According to FTIR spectroscopy (Fig. 2A), characteristic absorption peaks of ART, namely the carbonyl bond at 1,738 cm^{-1} and the peroxy bridge at 724 cm^{-1}[25], was observed in TA-Fe/ART@ZIF nanoparticles, indicating that ART was successfully encapsulated in the

nanoparticles. Next, the results of the thermogravimetric analysis revealed that Art completely abolished when the temperature was increased to approximately 400°C (Fig. 2B). Compared with the TA-Fe/ZIF nanoparticles, it was found that ART accounts for 7.1% of the total weight of the TA-Fe/ART@ZIF nanoparticles, which is basically consistent with the results of the HPLC analysis.

The results of TEM showed that ZIF-8 and ART@ZIF exhibited a similar uniform hexagon configuration and the particle size distribution was determined at approximately 100 nm (Fig. 3A and 3B). TA-Fe/ART@ZIF nanoparticles exhibited a spherical configuration and the particle size distribution was 150 nm. Compared with complete ART@ZIF, TA-Fe/ART@ZIF coated with Fe^{2+} and TA demonstrated an obvious conventional core-shell structure, and the size of the TA-Fe membrane was approximately 30 nm (Fig. 3A). Moreover, we performed area-elemental mapping on the analysis of the formed nanoparticles. The area-elemental mapping confirmed that the periphery of TA-Fe/ART@ZIF nanoparticles were encircled by Fe element to determine whether ART@ZIF had been successfully cloaked with $Fe^{2+}$and TA (Fig. 3B). By increasing the amount of added Fe^{2+}, we found that the hydrodynamic diameter of TA-Fe/ART@ZIF nanoparticles was increased (Fig. 1s). To further confirm the coating, we measured the zeta potential of various nanoparticles. The formation TA-Fe layer on ART@ZIF particles shifted the surface zeta from +21 mV potential to –19.5 mV due to the acidic nature of TA. (Fig. 2s).

Release and cytotoxicity of TA-Fe/ART@ZIF in vitro

Next, in order to study whether TA-Fe/ART@ZIF had pH-responsive decomposition behavior, we examined the release of ART from nanoparticles under neutral and acidic conditions. As shown in Fig. 4A, in the acidic PBS solution, the nanoparticles can rapidly release approximately 58% of ART within 1 h. However, under neutral conditions, the nanoparticles can only slowly release a minute amount of ART. In addition, during the treatment of the external solution of the dialysis membrane with external solution of the dialysis membrane with sodium hydroxide, the solution of the pH=5.0 group reacted with sodium hydroxide to produce a considerable white precipitate. However, this phenomenon was not observed in the pH=7.4 group.

According to our hypothesis, the white precipitate is a zinc hydroxide precipitate formed by the dissociation of zinc ions and alkali from the nanoparticles under acidic conditions. Collectively, this evidence successfully shows that our nanoparticles have the ability to dissociate under acidic conditions.

In the design of TA-Fe/ ART@ZIF nanosystem, the TA-Fe and ZIF structures are ablated to release the encased ART and Fe^{2+} under the acidic conditions of the tumor microenvironment. The upregulation of Fe^{2+} levels in cells would decompose Art into radicals through cleavage of the iron-mediated endoperoxide bridge, markedly enhancing the effects of ferroptosis. Accordingly, MTT assays were conducted to study the cytotoxicity of nanosystem to MDA-MB-231 cells and L929 cells. Compared with ART, TA-Fe/ ART@ZIF nanoparticles showed greater cytotoxicity to MDA-MB-231 cells (Fig. 4B) and low cytotoxicity to normal cells (Fig. 4C). TA-Fe/ ART@ZIF nanoparticles inhibited the activity of MDA-MB-231 cells by 53.9%, while Art at the same concentration inhibited only 24.1% of the whole cells. The

experimental results of calcein-AM staining confirmed that the quantity of viable MDA-MB-231 cells gradually descended with the increasing concentration of TA-Fe/ ART@ZIF nanoparticles. (Fig. 4D)

TA-Fe/ART@ZIF enhanced ROS generation in MDA-MB-231 cells

ART is known to exert its anticancer activity via generation of ROS produced by iron-mediated cleavage of the endoperoxide bridge.[26,27] Therefore, we have examined the efficiency of TA-Fe/ ART@ZIF to induce ROS generation by the 2',7'-dichlorodihydrofluorescein diacetate (DCHF-DA) probe. As shown in Fig. 5, the slightly stronger fluorescence signal was observed in cells treated with ART and TA-Fe/ZIF compared with untreated groups, indicating the ART and Fe^{2+} ions could induce ROS generation. By contrast, strong fluorescence signal exposure to TA-Fe/ ART@ZIF nano-drug is found in cells as an evidence of desired ROS yield. The ROS generation by endoperoxide of ART was mediated Fe^{2+}. The as-prepared nanosystem in cells would be degradated and make accumulation of Fe^{2+}, remarkably enhanced ROS generation.

The anticancer effect of ART and its derivatives has been attributed to their ability to induce apoptosis by various cellular processes, ranging from DNA damage response, the lysosome-mediated catabolic process macroautophagy, and oxidative stress.[13,26,28] And it was also reported that the iron-mediated cleavage of the endoperoxide bridge in ART could affect the intracellular oxidative balance to ferroptosis in many types of cancer cells.[11] This induction of ferroptosis based on oxidative imbalance can be further amplified with the addition of Fe^{2+}. While Fe^{2+} activates ART, it can also react with intracellular hydrogen peroxide to generate hydroxyl free radicals through the Fenton reaction, which enhances the apoptosis-inducing effect of ART in tumor cells.

TA-Fe/ART@ZIF induced apoptosis and ferroptosis in MDA-MB-231 cells

Meanwhile, to investigate that cell death and role of Fe^{2+}, we utilized iron chelator deferoxamine, apoptosis inhibitor Z-VAD-FMK, and ferroptosis inhibitor ferrostatin-1 to rescue these cells. As predicted, deferoxamine, a scavenger of Fe^{2+}, could obviously block cell death, suggesting the important role of Fe^{2+}. Moreover, the survival rate of MDA-MB-231 cells was significantly improved by apoptosis and ferroptosis inhibitor from 31.4% to 56.3% and 76.0%, respectively (Fig. 6A), highlighting the potential importance of apoptosis and ferroptosis in TA-Fe/ART@ZIF nanoparticles mediated cell death. In addition, we employed Annexin V- FITC based assay through flow cytometry, to quantitatively determine the degree of apoptosis. The results state that TA-Fe/ART@ZIF nanoparticles can induce apoptosis in 21.8% of MDA-MB-231 cells (Fig. 3s). This percentage was higher than that recorded for ART, implied that apoptosis is involved in the TA-Fe/ART@ZIF nanoparticles mediated, but it is not the main cause.

A common feature of ferroptosis is endogenous lipid peroxidation.[29] MDA, a prouduct of lipid peroxidation[30], was investigated to assess the degree of ferroptosis. Results showed TA-Fe/ART@ZIF nanoparticles produced approximately 2.5 times higher MDA levels than control group (Fig. 6B). This was presumed due to the presence nanocarrier-enriched Fe^{2+} and the corresponding elevation of lipid radicals levels. As one of the major antioxidant components in the cells, intracellular GSH is decreased

accompanied with ferroptosis.[31] Considering the import role of GSH in ferroptosis, we evaluated intracellular GSH level after treatment with TA-Fe/ART@ZIF nanoparticles. GSH was decreased significantly compared to vehicle-treated cells (Fig. 6C). This provided strong evidence for the depletion of GSH and oxidation imbalance, which was centered on the Fe^{2+} mediated activation of ART by TA-Fe/ART@ZIF nanoparticles. Next, western blotting was performed to understand the impact of TA-Fe/ART@ZIF nanoparticles. on GPX4 activity.[32] We observed that TA-Fe/ART@ZIF nanoparticles. caused a more significantly inhibition of GPX4 activity than did ART (Fig. 6D). These data also agreed well with the highest extent of GSH depletion. Although we have successfully demonstrated that TA-Fe/ART@ZIF nanoparticles can induce apoptosis/ferroptosis in TNBC cell lines, the antitumor effects of ART nanoparticles in tumor-bearing mice and the performance of ART nanoparticles in the field of metal imaging should be further investigated.

Conclusion

In summary, we designed metal (Fe^{2+})-phenolic (TA) coordination -coated on metal-organic framework MOF-wrapped ART nanoparticles to target TNCB cells through the synergism of apoptosis/ferroptosis. This method may provide new ideas and options for anti-tumor treatments, which are currently ineffective through traditional approaches.

Abbreviations

MOF: Metal organic frameworks; TNBC: triple-negative breast cancer

ART: artemisinin; TA: tannic acid; ZIF: zeolitic imidazolate framework-8

TA-Fe/ART@ZIF: tannic acid and ferrous ion-coated on the zeolitic imidazolate framework-8 with artemisinin encapsulated;

ROS: Reactive oxygen species; LPO: lipid hydroperoxides; GSH: glutathione;

TEM:Transmission electron microscopy;

FTIR: Fourier transform infrared spectroscopy;

HPLC: High-performance liquid chromatography; PBS :phosphate-buffered saline;

MTT: 3-(4, 5-Dimethylthiazol-2-yl)- 2,5-diphenyltetrazolium bromide;

DFO: deferoxamine; Fer-1:ferrostatin-1;

Z-VAD-FMK: N-benzyloxycarbonyl-Val-Ala-Asp(O-Me) fluoromethyl ketone;

Calcein-AM: Calcein-acetoxymethyl;

DCFH-DA: dichloro-dihydro-fluorescein diacetate; MDA: Malondialdehyde;

BSA：bovine serum albumin; TBST：Tris Buffered saline Tween;

SDS-PAGE: polyacrylamide gel electrophoresis' GPX4: glutathione peroxidase 4

Declarations

Authors' Contributions:

Z. Li and X. Wu performed the experiments and drafted the manuscript. W. Wang prepared and characterized the nanoparticles. C.Gai performed the statistical design of experiments. This research was carried out under the instruction of W. Zhang, W. Li and D. Ding. All authors helped to correct and polish the manuscript and read and approved the final manuscript.

Funding

The present study was supported by the Projects of Medical and Health Technology Development Program in Shandong province (Grant No. 2019WS590) and Project of Shandong Province Higher Educational Science and Technology Program (Grant No. J18KA279).

Competing Interests

The authors declare that they have no competing interests.

References

1. Cao JY, Dixon SJ. Mechanisms of ferroptosis. *Cellular and Molecular Life Sciences* 2016; **73**(11): 2195-209.
2. Strzyz P. Iron expulsion by exosomes drives ferroptosis resistance. *Nature Reviews Molecular Cell Biology* 2020; **21**(1): 4-5.
3. Yang WS, Stockwell BR. Ferroptosis: Death by Lipid Peroxidation. *Trends in Cell Biology* 2016; **26**(3): 165-76.
4. Hassannia B, Vandenabeele P, Vanden Berghe T. Targeting Ferroptosis to Iron Out Cancer. *Cancer Cell* 2019; **35**(6): 830-49.
5. Lu B, Chen XB, Ying MD, He QJ, Cao J, Yang B. The Role of Ferroptosis in Cancer Development and Treatment Response. *Frontiers in Pharmacology* 2018; **8**(992).
6. Wang S, Liao H, Li F, Ling D. A mini-review and perspective on ferroptosis-inducing strategies in cancer therapy. *Chinese Chemical Letters* 2019; **30**(4): 847-52.
7. Bianchini G, Balko JM, Mayer IA, Sanders ME, Gianni L. Triple-negative breast cancer: challenges and opportunities of a heterogeneous disease. *Nature Reviews Clinical Oncology* 2016; **13**(11): 674-90.

8. Timmerman Luika A, Holton T, Yuneva M, et al. Glutamine Sensitivity Analysis Identifies the xCT Antiporter as a Common Triple-Negative Breast Tumor Therapeutic Target. *Cancer Cell* 2013; **24**(4): 450-65.
9. Yu H, Guo P, Xie X, Wang Y, Chen G. Ferroptosis, a new form of cell death, and its relationships with tumourous diseases. *Journal of Cellular and Molecular Medicine* 2017; **21**(4): 648-57.
10. Talman AM, Clain J, Duval R, Ménard R, Ariey F. Artemisinin Bioactivity and Resistance in Malaria Parasites. *Trends in Parasitology* 2019; **35**(12): 953-63.
11. Chen G-Q, Benthani FA, Wu J, Liang D, Bian Z-X, Jiang X. Artemisinin compounds sensitize cancer cells to ferroptosis by regulating iron homeostasis. *Cell Death & Differentiation* 2020; **27**(1): 242-54.
12. Tu Y. Artemisinin—A Gift from Traditional Chinese Medicine to the World (Nobel Lecture). *Angewandte Chemie International Edition* 2016; **55**(35): 10210-26.
13. Efferth T. From ancient herb to modern drug: Artemisia annua and artemisinin for cancer therapy. *Seminars in Cancer Biology* 2017; **46**: 65-83.
14. Letchmanan K, Shen S-C, Ng WK, Tan RBH. Application of transglycosylated stevia and hesperidin as drug carriers to enhance biopharmaceutical properties of poorly-soluble artemisinin. *Colloids and Surfaces B: Biointerfaces* 2018; **161**: 83-93.
15. Ren G, Chen P, Tang J, et al. In vivo and in vitro evaluation of dihydroartemisinin prodrug nanocomplexes as a nano-drug delivery system: characterization, pharmacokinetics and pharmacodynamics. *RSC Advances* 2020; **10**(29): 17270-9.
16. Liu R, Yu X, Su C, Shi Y, Zhao L. Nanoparticle Delivery of Artesunate Enhances the Anti-tumor Efficiency by Activating Mitochondria-Mediated Cell Apoptosis. *Nanoscale Research Letters* 2017; **12**(1): 403.
17. Hu M, Ju Y, Liang K, Suma T, Cui J, Caruso F. Void Engineering in Metal–Organic Frameworks via Synergistic Etching and Surface Functionalization. *Advanced Functional Materials* 2016; **26**(32): 5827-34.
18. Zhang S, Pei X, Gao H, Chen S, Wang J. Metal-organic framework-based nanomaterials for biomedical applications. *Chinese Chemical Letters* 2020; **31**(5): 1060-70.
19. Zhang Z, Sang W, Xie L, Dai Y. Metal-organic frameworks for multimodal bioimaging and synergistic cancer chemotherapy. *Coordination Chemistry Reviews* 2019; **399**: 213022.
20. Wu M-X, Yang Y-W. Metal–Organic Framework (MOF)-Based Drug/Cargo Delivery and Cancer Therapy. *Advanced Materials* 2017; **29**(23): 1606134.
21. Kim K, Lee S, Jin E, et al. MOF × Biopolymer: Collaborative Combination of Metal–Organic Framework and Biopolymer for Advanced Anticancer Therapy. *ACS Applied Materials & Interfaces* 2019; **11**(31): 27512-20.
22. Zhang L, Wan S-S, Li C-X, Xu L, Cheng H, Zhang X-Z. An Adenosine Triphosphate-Responsive Autocatalytic Fenton Nanoparticle for Tumor Ablation with Self-Supplied H2O2 and Acceleration of Fe(III)/Fe(II) Conversion. *Nano Letters* 2018; **18**(12): 7609-18.

23. Rahim MA, Björnmalm M, Suma T, et al. Metal–Phenolic Supramolecular Gelation. *Angewandte Chemie International Edition* 2016; **55**(44): 13803-7.
24. Hoop M, Walde CF, Riccò R, et al. Biocompatibility characteristics of the metal organic framework ZIF-8 for therapeutical applications. *Applied Materials Today* 2018; **11**: 13-21.
25. Kapetanaki S, Varotsis C. Fourier Transform Infrared Investigation of Non-Heme Fe(III) and Fe(II) Decomposition of Artemisinin and of a Simplified Trioxane Alcohol. *Journal of Medicinal Chemistry* 2001; **44**(19): 3150-6.
26. Wong YK, Xu C, Kalesh KA, et al. Artemisinin as an anticancer drug: Recent advances in target profiling and mechanisms of action. *Medicinal Research Reviews* 2017; **37**(6): 1492-517.
27. Wang J, Zhang J, Shi Y, et al. Mechanistic Investigation of the Specific Anticancer Property of Artemisinin and Its Combination with Aminolevulinic Acid for Enhanced Anticolorectal Cancer Activity. *ACS Central Science* 2017; **3**(7): 743-50.
28. SINGH NP, LAI HC. Artemisinin Induces Apoptosis in Human Cancer Cells. *Anticancer Research* 2004; **24**(4): 2277-80.
29. Angeli JPF, Shah R, Pratt DA, Conrad M. Ferroptosis Inhibition: Mechanisms and Opportunities. *Trends in Pharmacological Sciences* 2017; **38**(5): 489-98.
30. Gai C, Yu M, Li Z, et al. Acetaminophen sensitizing erastin-induced ferroptosis via modulation of Nrf2/heme oxygenase-1 signaling pathway in non-small-cell lung cancer. *Journal of Cellular Physiology* 2020; **235**(4): 3329-39.
31. Xie Y, Hou W, Song X, et al. Ferroptosis: process and function. *Cell Death & Differentiation* 2016; **23**(3): 369-79.
32. Ursini F, Maiorino M. Lipid peroxidation and ferroptosis: The role of GSH and GPx4. *Free Radical Biology and Medicine* 2020; **152**: 175-85.

Figures

Figure 1

Schematic representation of preparation of TA-Fe/ART@ZIF nanoparticles and the synergistic induction of apoptosis/ferroptosis in tumor cells.

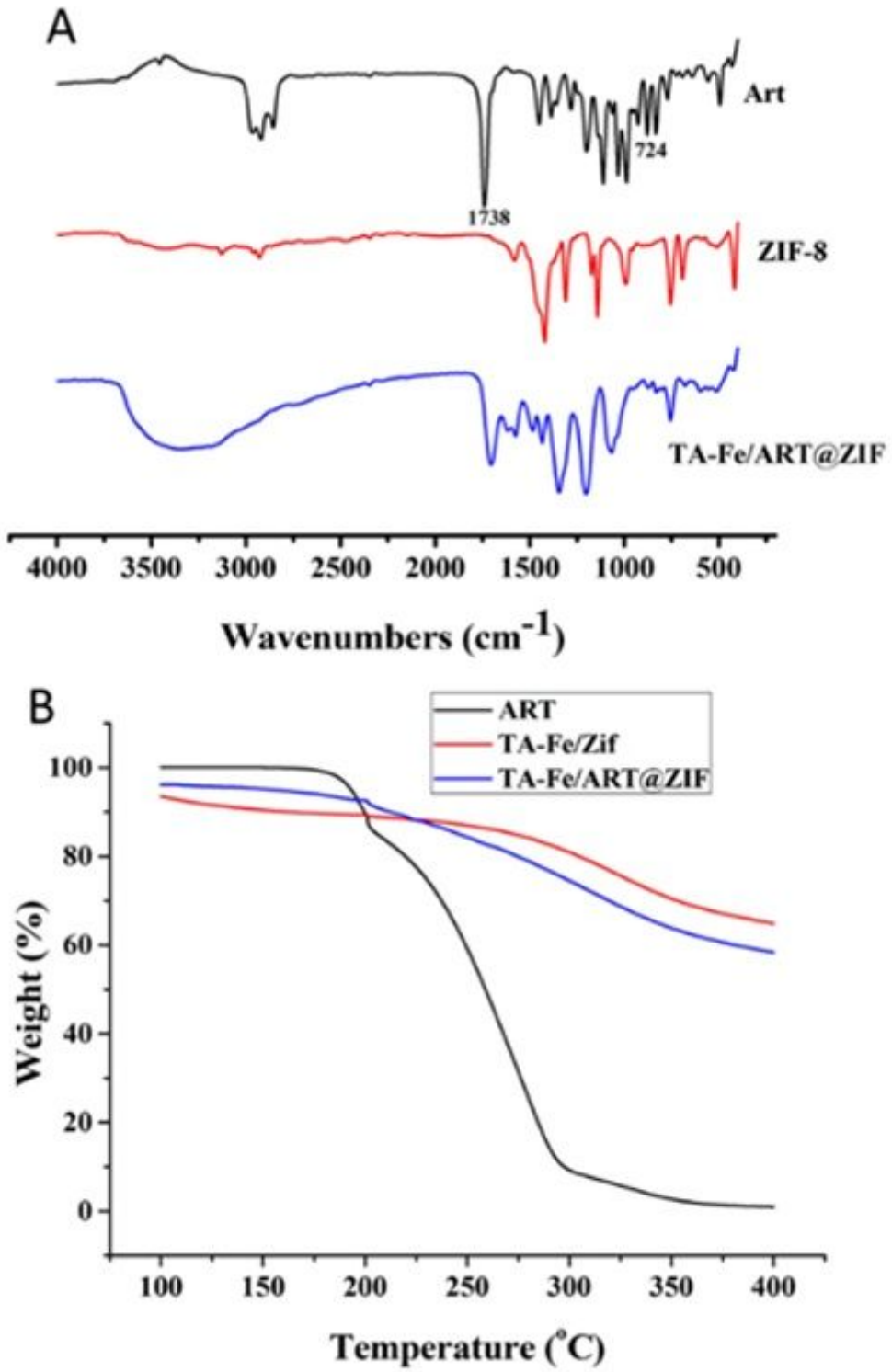

Figure 2

(A) FTIR of ART, ZIF-8 and TA-Fe/ART@ZIF; (B) Thermogravimetric analysis (TGA) of ART, TA-Fe/ZIF and TA-Fe/ART@ZIF

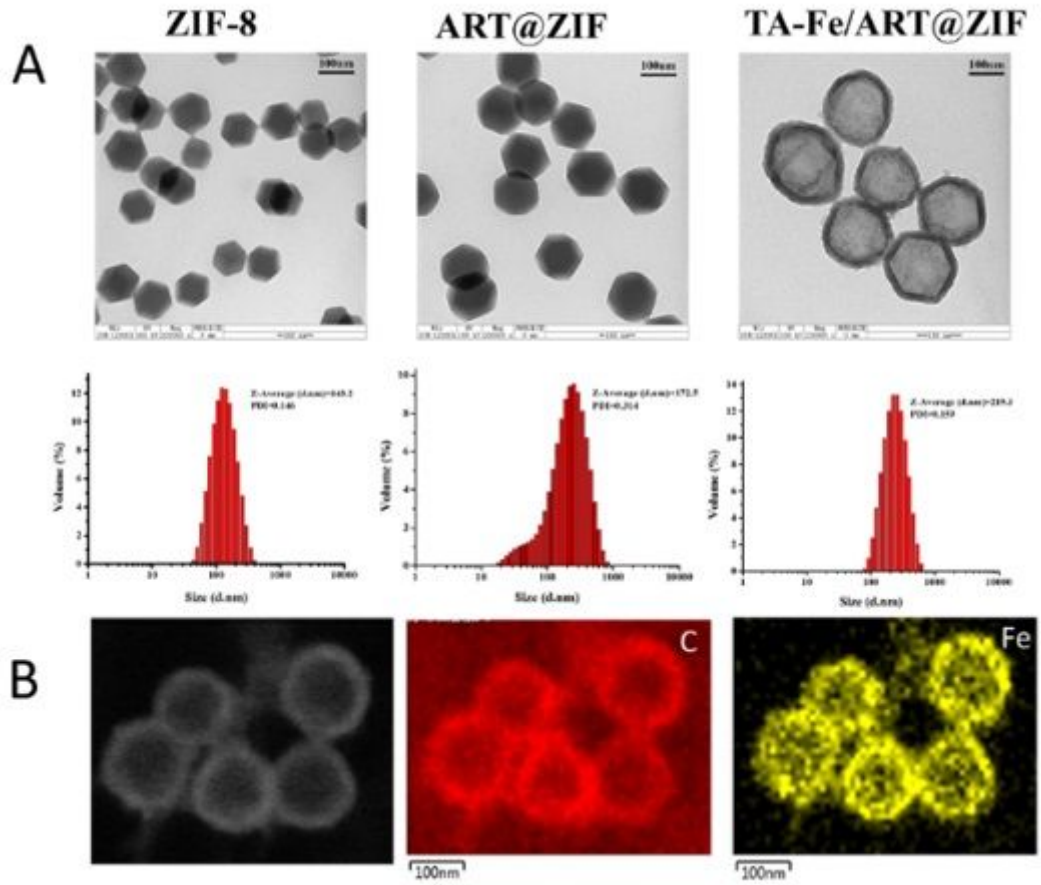

Figure 3

(A) TEM images and size distribution of ZIF-8, ART@ZIF and TA-Fe/ ART@ZIF nanoparticles. Scale bar: 100 nm; (B) Distribution of carbon and iron element in TA-Fe/ ART@ZIF nanoparticles. Scale bar: 100 nm.

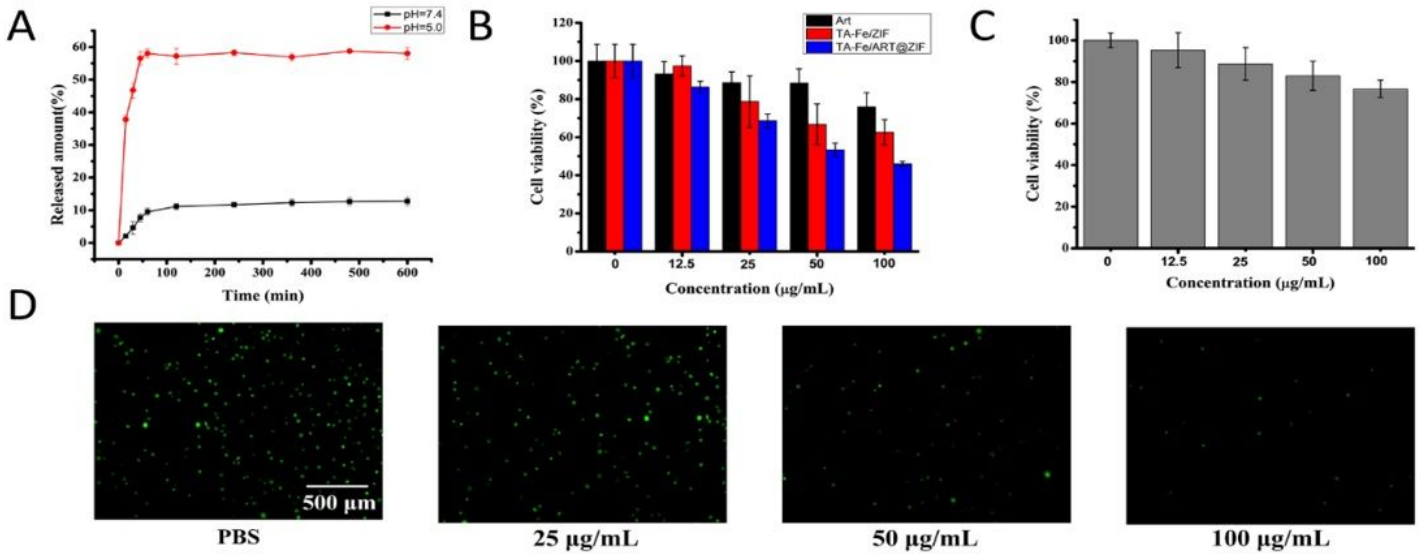

Figure 4

(A) In vitro release of ART from TA-Fe/ ART@ZIF nanoparticles in pH 7.4 and 5.0. (B) The cytotoxicity of ART, TA-Fe/ZIF and TA-Fe/ART@ZIF nanoparticles in MDA-MB-231 cells at 0, 12.5, 25, 50, and 100 μg/mL. (C) Viability of L929 cells treated with TA-Fe/ART@ZIF at different concentrations. (D) Calcein-AM staining of MDA-MB-231 cells treated with TA-Fe/ART@ZIF nanoparticles at concentrations of 0, 20, 50, and 100 μg/mL.

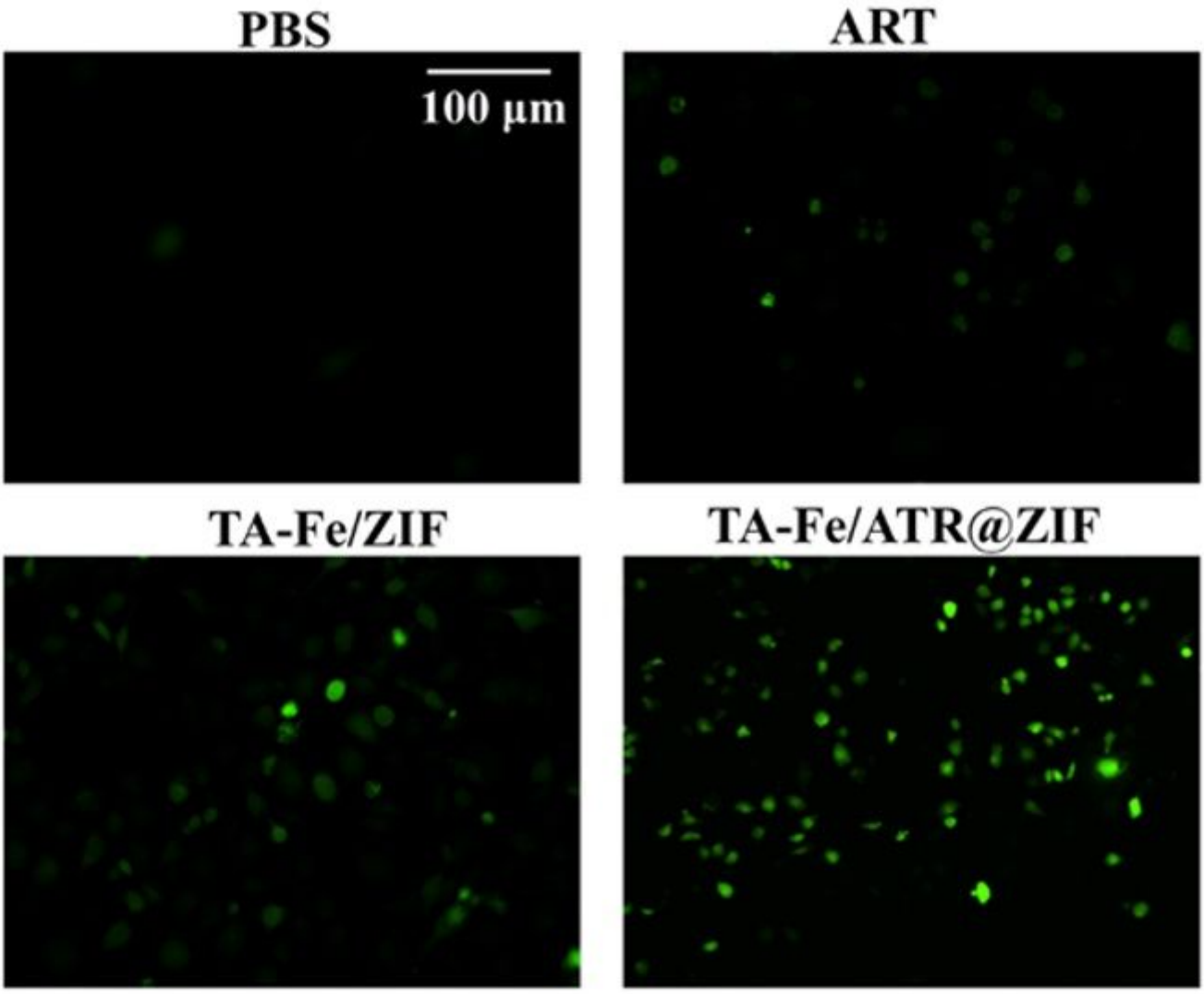

Figure 5

ROS production detected by fluorescence of DCFH-DA in MDA-MB-231 cells treated with ART, TA-Fe/ZIF and TA-Fe/ART@ZIF nanoparticles.

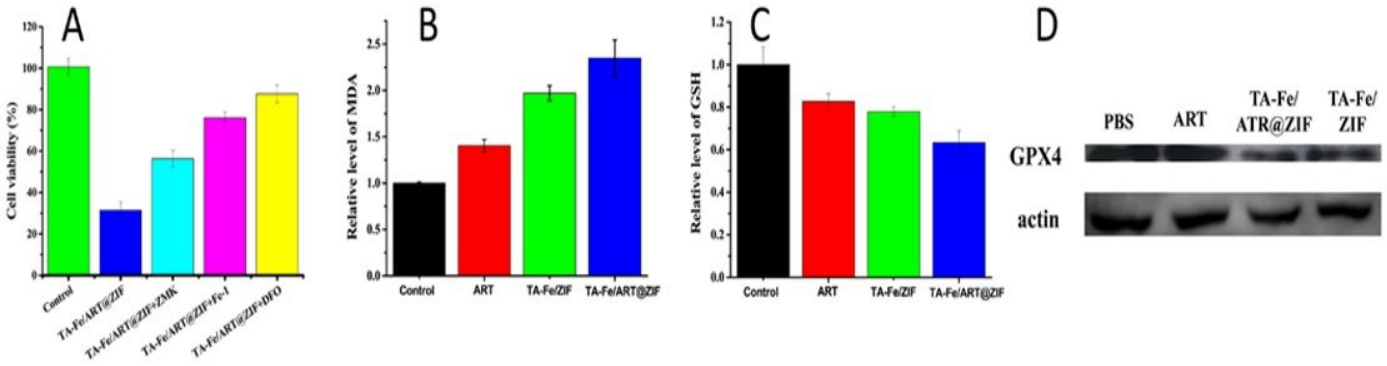

Figure 6

(A) Inhibitors DFO (deferoxamine), Fer-1 (Ferrostatin-1) and Z-VAD-FMK rescued the viability of MDA-MB-231 cells under treatment with 100 μg/mL TA-Fe/ART@ZIF nanoparticles, respectively. (B) ART, TA-Fe/ZIF and TA-Fe/ART@ZIF nanoparticles contributed to excessive MDA in MDA-MB-231 cells. (C) ART, TA-Fe/ZIF and TA-Fe/ART@ZIF nanoparticles consumed intracellular GSH. (D) The expression levels of GPX4 proteins in MDA-MB-231 cells. treated with ART, TA-Fe/ZIF and TA-Fe/ART@ZIF nanoparticles.

Supplementary Files

This is a list of supplementary files associated with this preprint. Click to download.

- supplement1.docx